Theor Chem Acc (2014) 133:1423
DOI 10.1007/s00214-013-1423-z

REGULAR ARTICLE

The mechanism of the cycloaddition reaction of 1,3-dipole molecules with acetylene: an investigation with the unified reaction valley approach

Marek Freindorf · Thomas Sexton · Elfi Kraka · Dieter Cremer

Received: 10 September 2013 / Accepted: 12 November 2013

Abstract The unified reaction valley approach (URVA) is used in connection with a dual-level approach to describe the mechanism of ten different cycloadditions of 1,3-dipoles XYZ (diazonium betaines, nitrilium betaines, azomethines, and nitryl hydride) to acetylene utilizing density functional theory for the URVA calculations and CCSD(T)-F12/aug-cc-pVTZ for the determination of the reaction energetics. The URVA results reveal that the mechanism of the 1,3-dipolar cycloadditions is determined early in the van der Waals range where the mutual orientation of the reactants (resulting from the shape of the enveloping exchange repulsion spheres, electrostatic attraction, and dispersion forces) decides on charge transfer, charge polarization, the formation of radicaloid centers, and the asynchronicity of bond formation. All cycloadditions investigated are driven by charge transfer to the acetylene LUMO irrespective of the electrophilic/nucleophilic character of the 1,3-dipole. However, an insufficient charge transfer typical of an electrophilic 1,3-dipole leads to a higher barrier. Energy transfer and energy dissipation as a result of curvature and Coriolis couplings between vibrational modes lead to an unusual energy exchange between just those bending modes that facilitate the formation of radicaloid centers. The relative magnitude of the reaction barriers and reaction energies is rationalized by determining reactant properties, which are responsible for the mutual polarization of the reactants and the stability of the bonds to be broken or formed.

Keywords Unified reaction valley approach · 1,3-Dipolar cycloadditions · Reaction mechanism · Mutual polarization · Energy transfer and dissipation

1 Introduction

1,3-Dipolar cycloadditions are pericyclic reactions leading to five-membered rings with heteroatoms [1–5]. The reactions involve a 1,3-dipole molecule and a reaction partner with a multiple bond as a dipolarophile. The reaction mechanism is in most cases concerted and stereo- and regiospecific with regard to both 1,3-dipole and dipolarophile. The interest in these cycloadditions results from the fact that a large variety of 1,3-dipole molecules XYZ rapidly reacts in an exothermic fashion to the desired cycloaddition product yielding a wealth of heterocycles. A suitable combination of groups X, Y, and Z containing C, N, or O leads to 18 different 1,3-dipole molecules, 12 of which are N-centered and 6 are O-centered. The XYZ framework of a 1,3-dipole molecule can contain 16 valence electrons as in the case of the diazonium betaines **1**, **2**, and **3** or the nitrilium betaines **4**, **5**, and **6** of Fig. 1. Alternatively, XYZ may have a total of 18 valence electrons as in the case of the azomethines **7**, **8**, and **9** of Fig. 1.

1,3-Dipole molecules are better described by resonance structures rather than simple Lewis structural formulas

Dedicated to Professor Thom Dunning and published as part of the special collection of articles celebrating his career upon his retirement.

Electronic supplementary material The online version of this article (doi:10.1007/s00214-013-1423-z) contains supplementary material, which is available to authorized users.

M. Freindorf · T. Sexton · E. Kraka (✉) · D. Cremer (✉)
Computational and Theoretical Chemistry Group (CATCO), Department of Chemistry, Southern Methodist University, 3215 Daniel Ave, Dallas, TX 75275-0314, USA
e-mail: ekraka@gmail.com

D. Cremer
e-mail: dieter.cremer@gmail.com

Published online: 04 December 2013

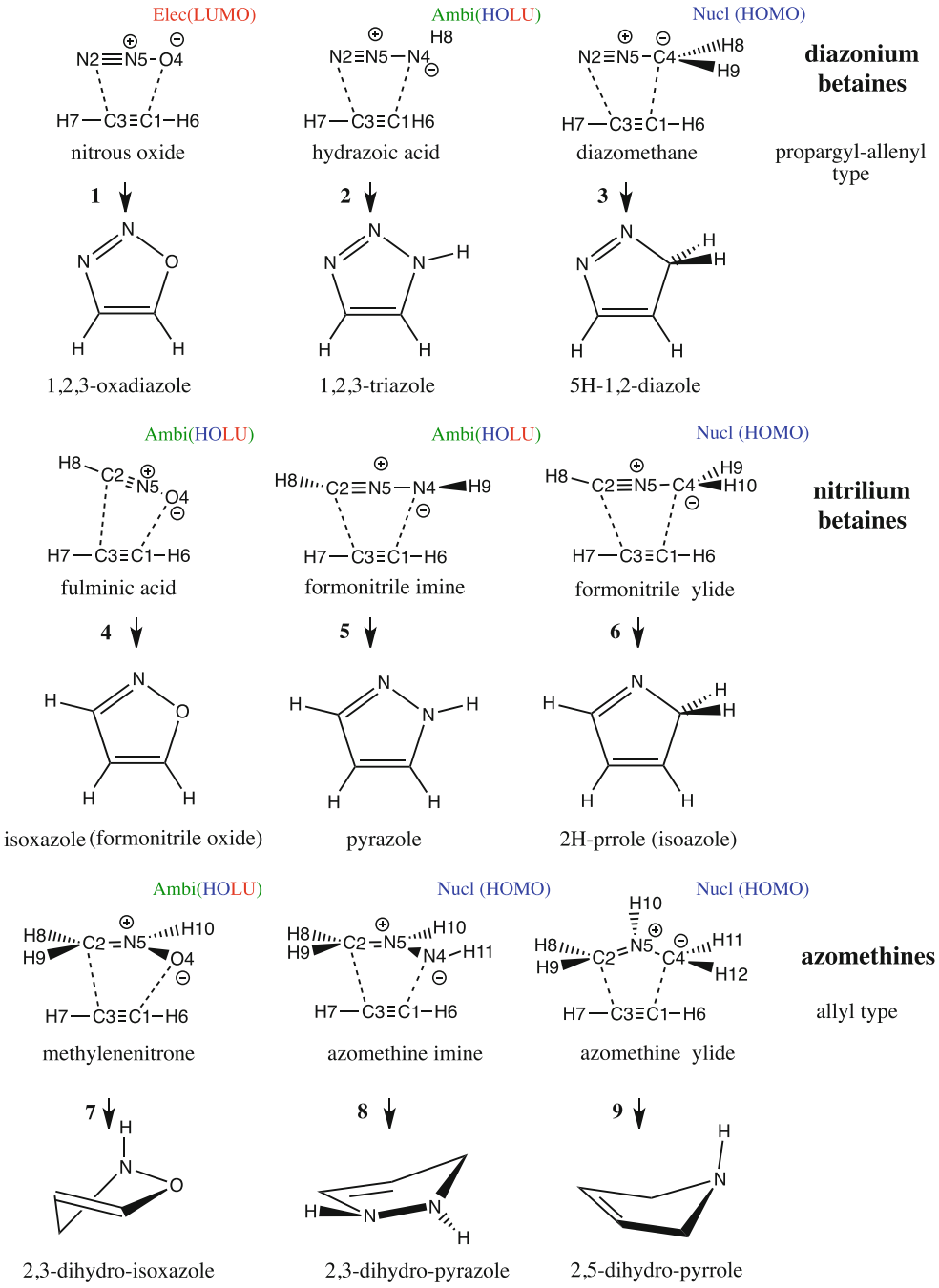

Fig. 1 1,3-Dipolar cycloaddition systems **1**–**9** investigated in this work. The name of the 1,3-dipole and the five-membered ring formed is given

with standard single, double, or triple bonds. The propargyl-allenyl-type resonance structures (only the former is shown in Fig. 1) are typical of the 16 valence electrons systems **1**–**6**, and the allyl-type resonance structures (only one shown) are typical of the N-centered 18 valence electron systems **7**–**9**. Although the electronic structures of the 1,3-dipole molecules are different, the mechanism of their cycloadditions to dipolarophiles is similar as reflected by their exothermicity, similar reaction barriers, and a similar stereochemistry [1–5]. This has been explained to some part by applying the Woodward–Hoffmann rules [6] and identifying 1,3-dipolar cycloadditions as concerted, symmetry-allowed pericyclic $\pi^4 s + \pi^2 s$ reactions involving 4 π-electrons of the 1,3-dipole and 2 π-electrons of the double or triple bond of the dipolarophile leading in this way to a Hückel-aromatic, stabilized transition state (TS) according to the Evans–Dewar–Zimmerman rules [7]. The state- and orbital-symmetry analysis can explain the relatively low barriers of 1,3-dipolar cycloadditions and their stereochemistry. Detailed trends in reaction rates and changes in the stereochemistry have been explained, often with success, on the basis of frontier orbital theory [8]. An

even more detailed insight has been provided by a large number of quantum chemical investigations [9–21] where especially the thorough and extensive work of Houk et al. [22–37] has to be mentioned.

1,3-Dipolar cycloadditions are versatile tools for the synthesis of heterocyclic molecules [1–5]. Applications range from asymmetric organic synthesis [38, 39], catalysis [40–43], materials science [44], and drug design [45] to chemical biology [46, 47]. The mechanism of the 1,3-dipolar cycloaddition reactions had been controversially debated starting in the late 1960s when Huisgen [48] postulated a concerted mechanism and Firestone [49] advocated a stepwise biradical mechanism. Numerous quantum chemical investigations have been performed since then to shed light on the mechanism of 1,3-dipolar cycloadditions [33, 50, 51], to provide accurate energetic data [29, 34–36] and kinetic data [24], and to investigate the regioselectivity of these reactions [9, 11, 17, 28]. Calculations could solve the Huisgen–Firestone controversy; the concerted mechanism is favored for the reactions of the unsubstituted 1,3-dipoles with ethylene and acetylene [21, 26, 27], whereas the stepwise mechanism becomes likely when the 1,3-dipoles and dipolarophiles are substituted by radical-stabilizing groups [25, 31, 52].

Still, open mechanistic questions concern the driving force of the cyclization and the electronic factor(s) that determine(s) the barrier height. Currently, three different rate-determining factors are discussed in the literature: (1) the *distortion energy* of dipole and dipolarophile as defined by Houk et al. [22, 23, 30, 32]; (2) reaction acceleration by an excitation of the *bending vibrations* of the 1,3-dipole [13, 14, 26, 27]; and (3) the *biradical character* of the 1,3-dipole molecule [10, 12].

Most of the previous work on the 1,3-dipolar cycloadditions has focused on finding a rationale for the relatively low reaction barriers because they predominantly determine the reaction rate and the yield of a given product. A general assumption in this connection is that the similarity of the activation energies indicates a similarity of the reaction mechanism.

In this work, we will show that comparable reaction barriers do not necessarily imply a similarity in the reaction mechanism. Conversely, two reactions may have a similar mechanism although they have different barriers. We approach the question of the mechanism of the 1,3-dipolar cycloadditions in a different way than previous investigations by utilizing the unified reaction valley approach (URVA) of Kraka and Cremer [53–57]. URVA explores the reaction path and the reaction valley via its direction and curvature, using a number of tools that provide direct information about the reaction mechanism. According to a definition two of us have given recently [53], the mechanism of a reaction is determined by the nature and sequence of elementary electronic events that take place in each phase of the reaction starting from the first long-range interactions between the reactants in the entrance channel and terminating with the finalization of the products in the exit channel.

We will show that the fate of the reaction is determined early on in the van der Waals region of the entrance channel. Furthermore, we will reveal that all 1,3-dipolar cycloadditions investigated in this work pass through the same reaction phases; however, there are distinct differences between different classes of cycloadditions. Also, it will become apparent that there is a difference between reactions with radicaloid and biradicaloid character and that the dipolarophile rather than the 1,3-dipole initiates bond formation.

The current investigation is based on a detailed analysis of the reaction path and the reaction valley, which will lead to a better understanding of the mechanism than it is possible with a conventional mechanistic analysis based on the features of the stationary points along the reaction path. Our focus will be on well-defined transient points along the reaction path corresponding to bond breaking and bond formation, rehybridization, and (bi)radicaloid formation.

The results of this work are presented in the following way. In Sect. 2, the computational methods used in this work are described. The results of the quantum chemical investigation of ten 1,3-dipolar cycloadditions are presented and discussed in Sect. 3. Conclusions will be drawn in the final section.

2 Computational methods

The current investigation is based on URVA [53–57], the reaction path Hamiltonian of Miller, Handy, and Adams [58], and the local vibrational mode description of Konkoli and Cremer [59–62] recently theoretically justified by Zou and Cremer [63, 64]. URVA has been repeatedly described in previous publications [55, 65–69] as well as several review articles [53, 54, 56, 57]. Therefore, we refrain from a detailed account of the theory of URVA and the use of local vibrational modes and instead outline the methods used in a more qualitative fashion.

Each 1,3-dipolar cycloaddition system is investigated with a dual-level approach: (1) A high level such as CCSD(T)-F12/aug-cc-pVTZ [70–72] is used to determine the energetics of the reaction from the relative energies (enthalpies) of the stationary points along the reaction path. (2) The reaction valley and the reaction path embedded in the reaction valley are calculated at a lower level using density functional theory (DFT). The primary objective of URVA is to determine those locations along the reaction path at which the chemical processes of bond breaking and forming take place, where the first van der Waals interactions lead to chemical change, where rehybridization leads

to the formation of radicaloid and biradicaloid structures, and where, after bond formation, the electrons are reorganized to form delocalized π-electron ensembles. To get these insights, a paradigm shift with regard to conventional mechanistic studies is made: The primary concerns are no longer the energy or geometry changes of the reaction complex, but rather the features of the reaction path, which can be directly related to changes in the electronic structure [53, 54, 56].

Chemical change and chemical processes always imply a curving of the reaction path [53, 54, 56]. If the reaction path becomes a straight line, physical processes driven exclusively by electrostatic forces take place with no or just a steady change in the electronic structure. Chemical processes are characterized by catastrophe points in the electron density distribution of the reaction complex (infinitesimal changes in the density lead, e.g., to singularity catastrophes in its topological structure reflecting sudden changes in bonding), and this in turn is connected with directional changes (curving) of the reaction path (which must not be confused with the energy curvature of the potential energy surface). Changes in the reaction path can be described with the help of the two Frenet vectors: path tangent (direction) and path curvature (curving). A third Frenet vector leading to the path torsion is only of relevance in case of repeated curving of the path over a larger area, which seldom occurs. The reaction complex and the reaction path are intimately related, and analyzing the latter on the basis of just two quantities (direction and curvature vector) solves the problem of monitoring of the 3N-L (N: number of atoms; L: number of translations and rotations) degrees of freedom of the reaction complex during the reaction.

The curvature vector *kappa* has the dimension of 3N–L. In URVA, the scalar curvature (the length of the curvature vector) is investigated to obtain an easy-to-analyze function $\kappa(s)$ (scalar curvature as a function of the mass-weighted arc length s; $s < 0$: entrance channel of the reaction; $s = 0$: TS; $s > 0$: exit channel). The square of the scalar curvature is equal to the sum of the squares of the normal mode curvature coupling coefficients $B_{\mu,s}$, which describe the coupling between the translational mode along the reaction path and the normal vibrational modes $\mathbf{l}_\mu$ spanning the reaction valley [58]. The normal vibrational modes, in turn, can be decomposed into the local vibrational modes $\mathbf{a}_n$ of Konkoli and Cremer [59, 60]. Each local mode is driven by an internal coordinate q_n of the reaction complex. By decomposing the scalar curvature into local mode curvature coupling coefficients $A_{n,s}$, those parts of the reaction complex can be directly identified, which are related to the curving of the reaction path and enhancements of the scalar curvature.

In this way, all electronic structure changes of the reaction complex along the reaction path can be monitored. They present the basis of the reaction mechanism, which develops in the form of a sequence of reaction phases along the reaction path. Each reaction phase is characterized by a curvature enhancement or peak enclosed by locations of minimal or even zero curvature [53, 54, 56]. The positions of minimal curvature correspond to transient structures of the reaction complex with interesting electronic structure features. Suitable changes of the reaction complex and/or the reaction environment can transform these transient points into stationary points, and therefore, the terms *hidden intermediate* and *hidden transition state* have been coined to describe the mechanistic relevance of these curvature minima [53, 65, 67].

There are three quantities, which are used in this work to describe the reaction mechanism as it develops via the scalar curvature function $\kappa(s)$: (1) local mode curvature coupling coefficients $A_{n,s}$ to describe the mechanism; (2) normal mode curvature coupling coefficients $B_{\mu,s}$ to describe energy transfer from the vibrational modes into the translational motion along the path; and (3) normal mode Coriolis (mode–mode) coupling coefficients $B_{\mu,\nu}$ to describe energy dissipation between the modes. Apart from this, URVA calculates charge transfer and charge polarization as a function of s and determines local mode force constants and frequencies of the reaction complex [63, 64].

For URVA, a representative reaction path must be chosen, which can be the intrinsic reaction coordinate (IRC) path of Fukui [73], a reasonable down-hill path, or any other representative path [68, 74]. In this work, we use the IRC path and follow it with an algorithm recently suggested by Hratchian and Kraka [75] where B3LYP/6-31G(d,p) [76–78] is used to describe the reaction valley. For each cycloaddition path, between 630 and 930 path points were calculated. At each second path point, generalized harmonic vibrational frequencies of the reaction complex were determined. Curvature, curvature coupling coefficients, and all other URVA-related quantities were calculated with the *ab initio* package COLOGNE13 [79]. The analysis of the charge distribution (charge transfer and charge polarization) was based on the natural bond orbital (NBO) method of Weinhold et al. [80, 81]. For the CCSD(T)-F12 calculations [71], the program package MOLPRO [82] was used. Reaction enthalpies $\Delta_R H(298)$, activation enthalpies $\Delta H^a(298)$, reaction free energies $\Delta_R G(298)$, and $\Delta G^a(298)$ were calculated using CCSD(T)-F12/aug-cc-pVTZ energies in connection with B3LYP/6-31G(d,p) or ωB97X-D/aug-cc-pVTZ geometries and vibrational frequencies [83, 84]. The latter functional is known to provide an improved description of dispersion interactions [83, 85]. Basis set superposition error (BSSE) corrections were obtained using the counterpoise method [86].

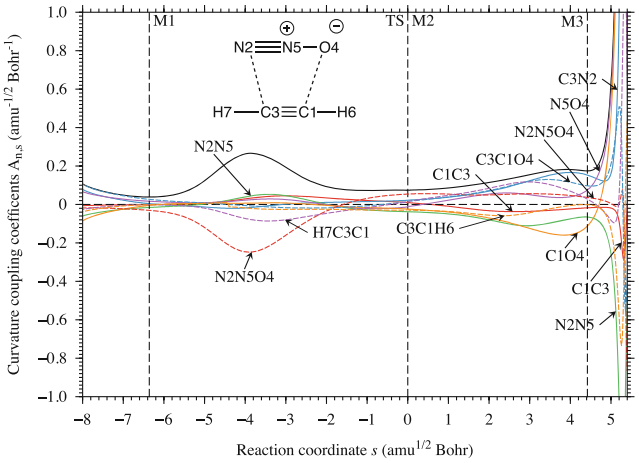

(a) Nitrous oxide, **1**

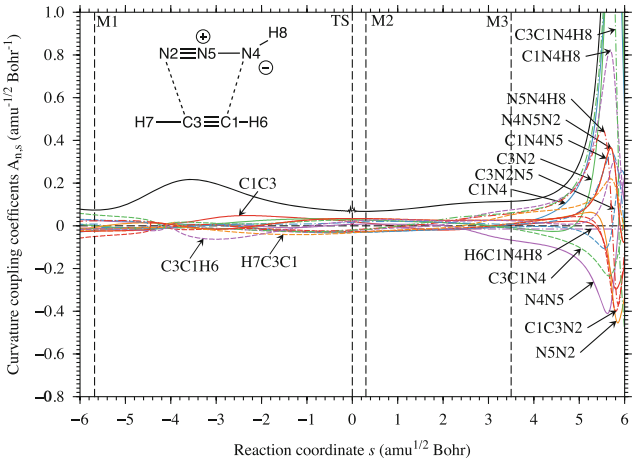

(b) Hydrazoic acid, **2**

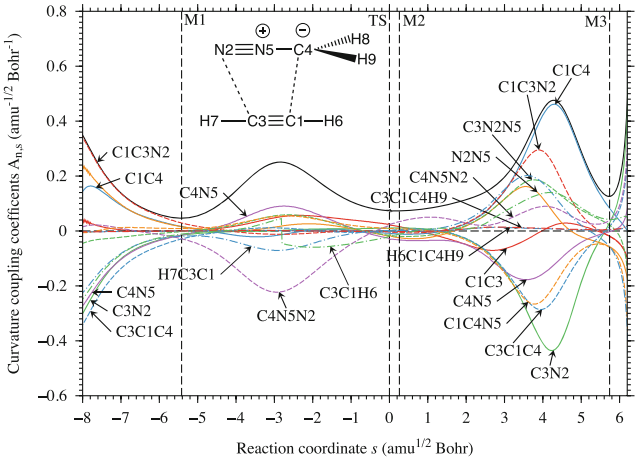

(c) Diazomethane, **3**

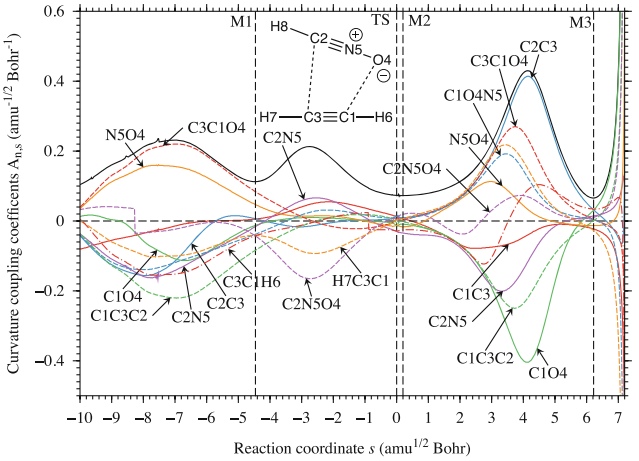

(d) Fulminic acid, **4**

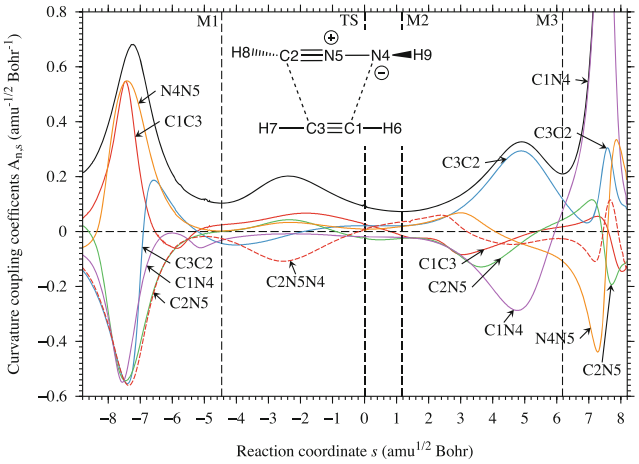

(e) Formonitrile imine, **5**

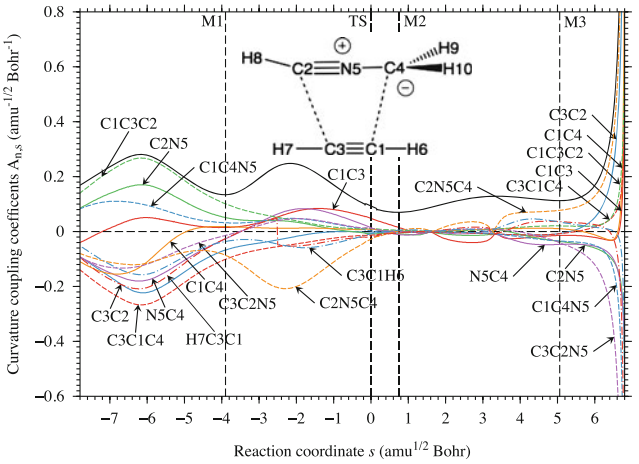

(f) Formonitrile ylide, **6**

Fig. 2 Scalar curvature as a function of the reaction path parameter s (*solid black line*) for 1,3-dipolar cycloaddition systems **1**–**10**. Local mode curvature coupling coefficients are given in *color*. The borders of the reaction phases are indicated by *vertical dashed lines* at curvature points M1, M2, and M3. The TS at $s = 0$ amu$^{1/2}$ Bohr is also indicated by a *vertical dashed line*. **a** Nitrous oxide, **1**, **b** hydrazoic acid, **2**, **c** diazomethane, **3**, **d** fulminic acid, **4**, **e** formonitrile imine, **5**, **f** formonitrile ylide, **6**, **g** methylene nitrone, **7**, **h** azomethine imine, **8**, **i** azomethine ylide, **9**, **j** nitryl hydride, **10**

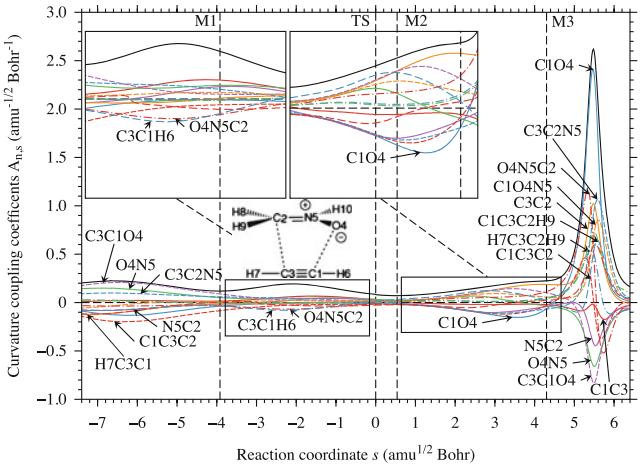

(g) Methylenenitrone, **7**

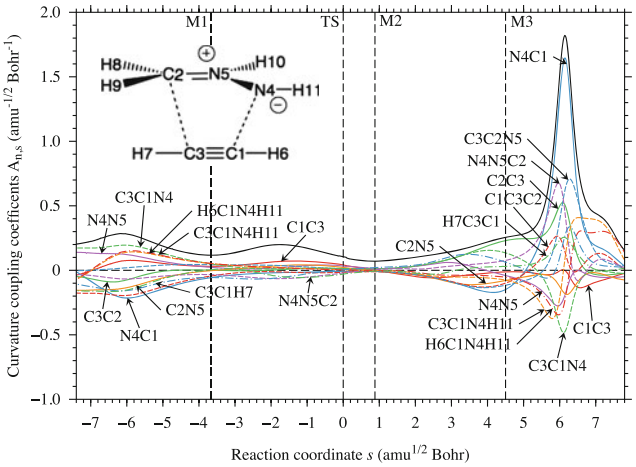

(h) Azomethine imine, **8**

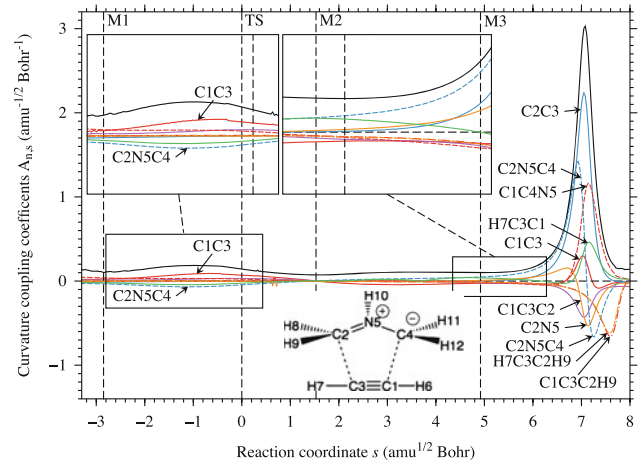

(i) Azomethine ylide, **9**

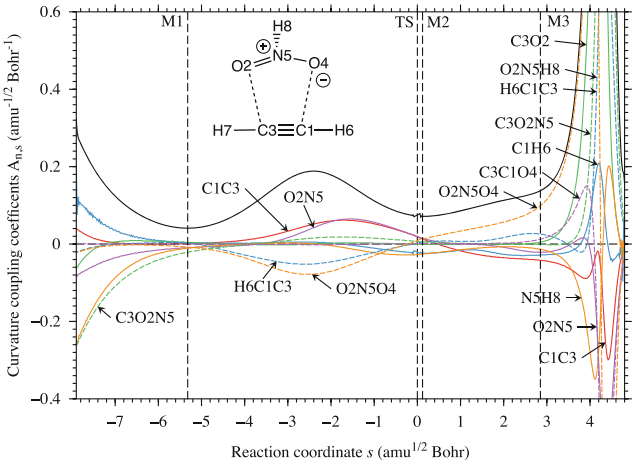

(j) Nitryl hydride, **10**

Fig. 2 continued

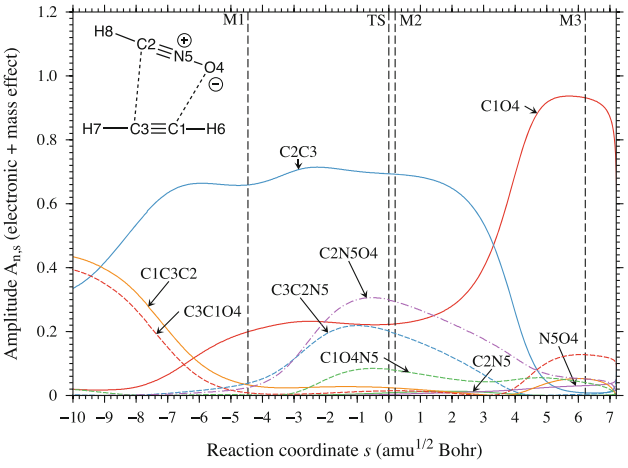

Fig. 3 Components of the reaction path direction given as a function of the reaction parameter s for reaction system **4**

3 Results and discussion

In Fig. 2, curvature diagrams $\kappa(s)$ of the 1,3-dipolar cycloaddition systems **1**–**9** listed in Fig. 1 and the nitryl hydride system **10** are shown, where each curvature is decomposed in terms of local mode curvature coupling coefficients $A_{n,s}(s)$. An example for the composition of the reaction path direction in terms of local mode contributions is given for reaction system **4** in Fig. 3 and the charge transfer from the 1,3-dipole to acetylene in Fig. 4a and b. Calculated energy barriers and reaction energies are analyzed in Figs. 5 and 6. An example of the dependence of the vibrational frequencies on the path parameter s is given in Fig. 7a and b for system **4**.

The energy data for the ten cycloaddition reactions investigated in this work are summarized in Table 1. The reaction and activation enthalpies obtained at the

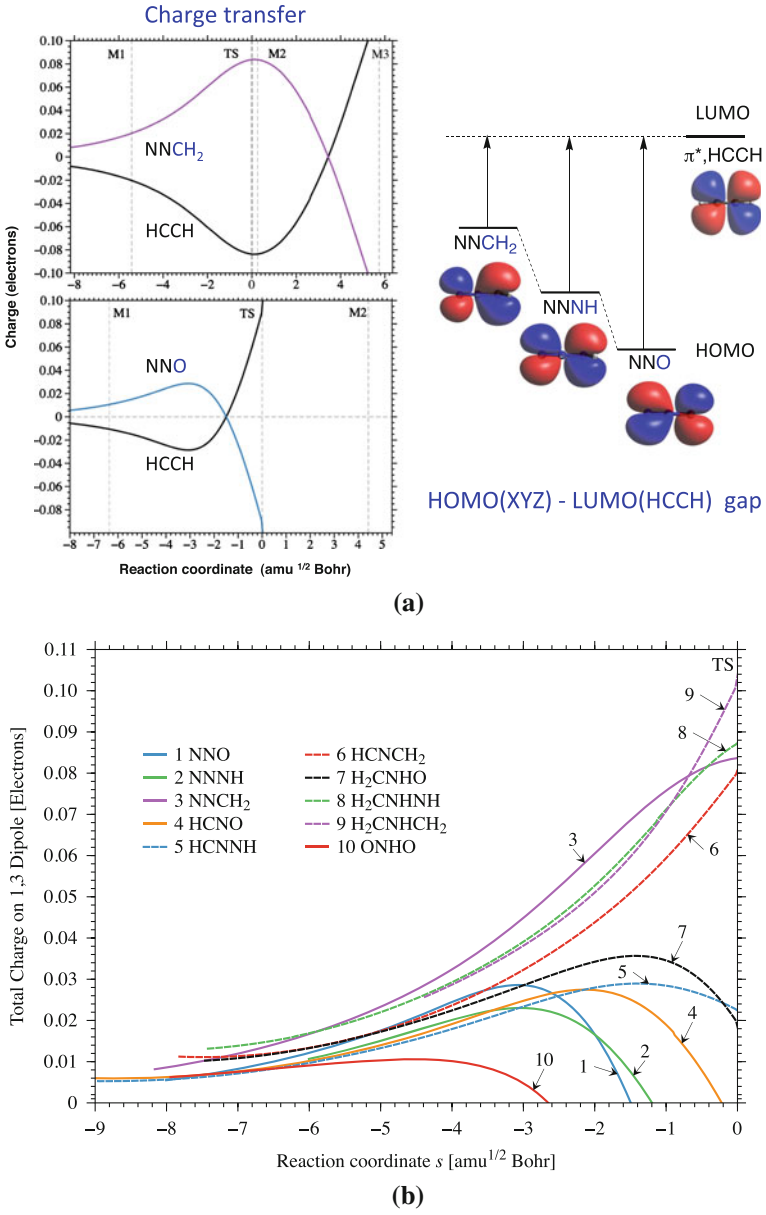

Fig. 4 **a** Charge transfer from the HOMO of the 1,3-dipole (schematically drawn for NNZ) to the LUMO of acetylene in the case of reaction systems **1**, **2**, and **3**. **b** Charge transfer from the 1,3-dipole to acetylene in the entrance channel (TS at $s = 0$ amu$^{1/2}$ Bohr) given as a function of the reaction parameter s

CCSD(T)-F12a/aug-cc-pVTZ level of theory compare well with the corresponding CBS-QB3 values of Houk et al. [30, 50]. The corresponding B3LYP and ωB97X-D results (after BSSE corrections) show a reasonable agreement with the CCSD(T)-F12a data, which makes them both suitable for the description of the reaction valley. To reduce the computational costs, B3LYP/6-31G(d,p) was used for the URVA analysis as described above. It is interesting to note that the entropy contributions $\Delta_R S(298)$ to the free reaction energies $\Delta_R G(298)$ are fairly constant (−36 to −41 entropy units, Table 1) as are the contributions $\Delta S^a(298)$ to the free activation energies, $\Delta G^a(298)$, which vary from −32 to −37 entropy units. The values collected in Table 1 suggest that entropy effects can be excluded from the discussion of the reaction mechanism.

All ten cycloaddition reactions follow a four-phase mechanism irrespective of the nature of the 1,3-dipole reacting with acetylene. These phases will be discussed below by making reference to the curvature diagrams presented in Fig. 2.

Reaction phase 1 (entrance channel from start to curvature point M1): There are four properties of the 1,3-dipole molecule, which are decisive in the first phase of the cycloaddition reaction:

1. The first property is the exchange repulsion envelope around the reactants, which decides on the approach mode. If one terminal group of the 1,3-dipole is more electronegative than the other, the exchange repulsion envelope at this end (e.g., an O atom) will be more

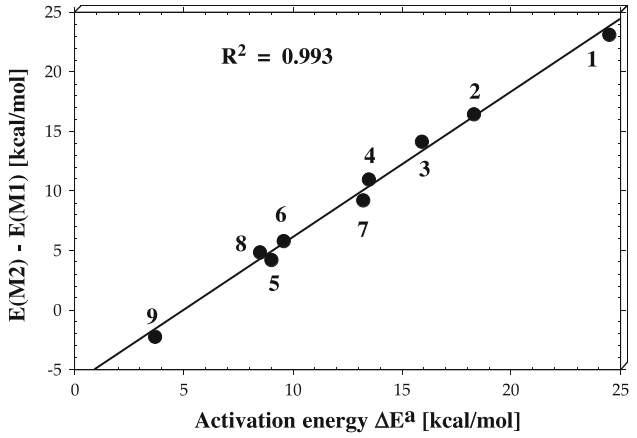

Fig. 5 Comparison of the energy change in reaction phase 2, E(M2) – E(M1), with the activation energy ΔE^a for the nine 1,3-dipolar cycloaddition reactions (for numbering of reaction complexes, see Fig. 1)

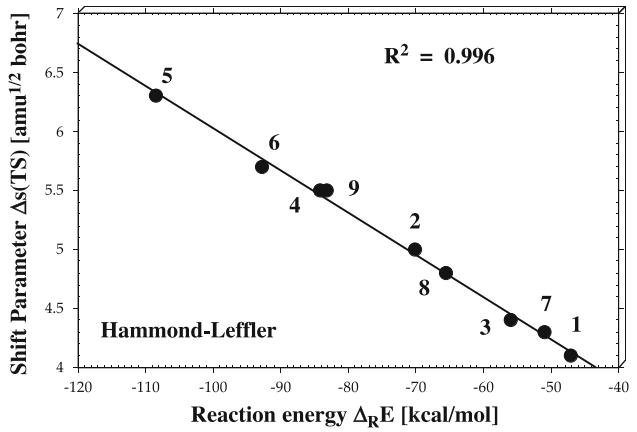

Fig. 6 Comparison of the parameter $\Delta s(TS)$, which determines the shift of the TS relative to the center M3 of the bond-forming processes, with the reaction energy $\Delta_R E$ for the nine 1,3-dipolar cycloaddition reactions (for numbering of reaction complexes, see Fig. 1). A positive $\Delta s(TS)$ value indicates an early TS according to the Hammond–Leffler postulate

contracted than at the other terminal group. The reactants will approach each other in such a way that stabilizing dispersion interactions and electrostatic attractions are maximized while minimizing the short-range exchange repulsion. The approach distance will be shorter for the more electronegative group than for the other group. Accordingly, there is a larger or smaller inclination angle of the axis of the 1,3-dipole molecule (when it is linear, otherwise the 1,3 connection axis) relative to the axis of acetylene. These are given in Table 2 for the first point in the entrance channel where interaction energies are smaller than just a few tenth of a kcal/mol.

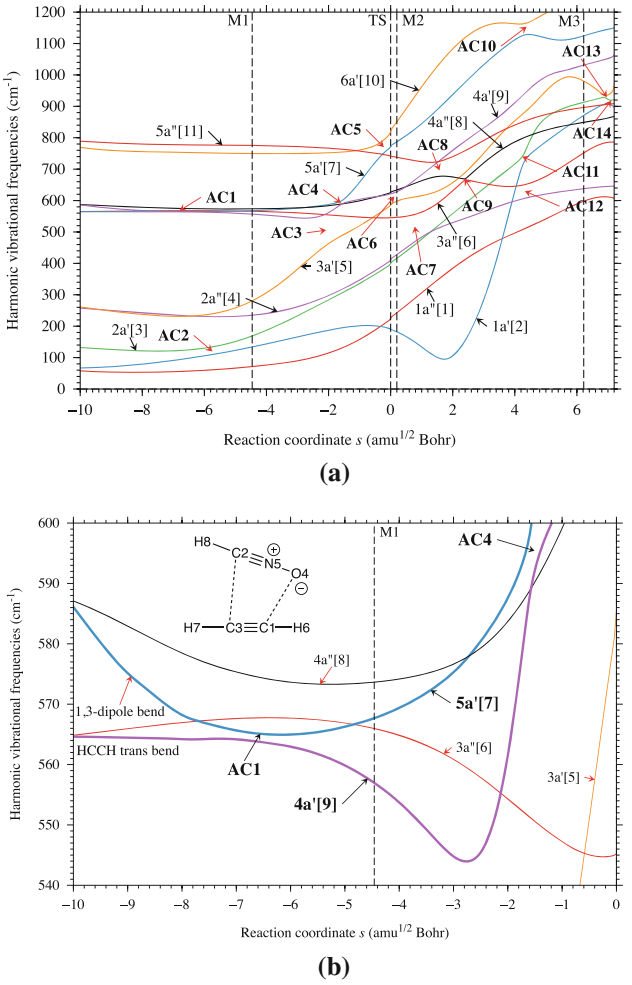

Fig. 7 Vibrational frequencies of reaction system **4** given as a function of the reaction parameter s. The avoided crossings (AC) are the positions of mode–mode (Coriolis) coupling leading to energy dissipation. **a** Framework vibrations. **b** 1,3-Dipole and acetylene bending

One can see that the eletronegativity difference between X2 and Z4 determines sign and magnitude of the inclination angle (Table 2). Systems with an electronegative group Z (**1**, **4**, **5**, **7**, and **8**; compared with Fig. 1) have a positive inclination angle, systems **3** and **6** have a negative inclination angle (i.e., the distance C3X2 is shorter than the distance C1Z4), whereas systems **2**, **9**, and **10** approach each other in a parallel fashion because of symmetry and/or similar (identical) electronegativities of X2 and Z4. The mode of approach has direct consequences for the sequence of bond formation as will be shown below.

2. The second property relevant to the mechanism is the dipole moment of the 1,3-dipole molecule, where only its component parallel to the axis of the approaching acetylene molecule matters. This has been determined

Table 1 Energetics of cycloaddition reactions **1–10**

System	$\Delta_R E$			ΔE^a			CCSD(T)-F12a		CBS-QB3		ωB97X-D		CCSD(T)-F12a	
	A	B	C	A	B	C	$\Delta_R H(298)$	$\Delta H^a(298)$	$\Delta_R H(298)$	$\Delta H^a(298)$	$\Delta_R S(298)$	$\Delta S^a(298)$	$\Delta_R G(298)$	$\Delta G^a(298)$
1 (NNO)	−44.1	−47.1	−42.3	30.2	24.5	27.5	−39.5	27.3	−38.8	26.7	−35.7	−31.6	−28.8	36.7
2 (NNNH)	−70.6	−70.1	−67.1	22.5	18.5	19.7	−63.1	20.0	−63.7	19.0	−40.2	−34.0	−51.1	30.2
3 ($NNCH_2$)	−56.9	−56.0	−56.8	17.4	15.9	14.3	−52.6	14.9	−51.2	14.0	−39.7	−34.0	−40.8	25.0
4 (HCNO)	−83.7	−84.2	−82.0	16.7	13.5	12.9	−77.5	13.0	−75.8	13.3	−38.5	−31.9	−66.0	22.5
5 (HCNNH)	−112.1	−108.4	−107.9	10.2	9.0	7.7	−102.1	8.1	−102.5	7.5	−41.2	−33.6	−89.8	18.1
6 ($HCNCH_2$)	−96.2	−92.8	−95.3	9.2	9.6	6.3	−90.3	6.8	−88.8	6.5	−41.4	−33.9	−77.9	16.9
7 (H_2CNHO)	−52.0	−51.0	−50.3	14.7	13.2	13.0	−46.5	13.8	−45.6	12.9	−39.8	−36.4	−34.7	24.7
8 (H_2CNHNH)	−69.6	−65.6	−66.4	8.4	8.6	1.0	−62.2	7.7	−61.3	6.5	−40.0	−36.2	−50.3	18.5
9 (H_2CNHCH_2)	−87.0	−83.2	−84.7	1.9	3.8)	1.1	−79.9	1.8	−79.0	0.4	−38.5	−34.3	−68.4	12.0
10 (ONHO)	−22.4	−23.8	−22.1	32.9	27.3	31.1	−19.3	31.4	−18.8	28.4	−38.3	−35.9	−7.9	42.1

Reaction energies and reaction barriers are given for A: ωB97X-D, B: B3LYP, and C: CCSD(T)-F12a. B3LYP calculations carried out with the 6-31G(d,p) basis set. All other calculations were carried out with the aug-cc-pVTZ basis set. Enthalpies and free energies were obtained with ωB97X-D geometries and thermochemical corrections. Energy differences are given in kcal/mol and entropy differences in cal/(mol K). CBS-QB3 reference data from Ref. [50]. Basis set superposition error corrections were obtained using the counterpoise method

for the first point in the entrance channel and is given in Table 2 as μ_z (the direction z is that defined by the acetylene CC axis) together with the total dipole moment of the 1,3-dipole. The magnitude of the dipole component μ_z reflects the ability of the 1,3-dipole to polarize the acetylene molecule. It has a direct influence on the barrier of the reaction.

3. The third property is the polarizability of the reactants. If one compares different dipolarophiles, one would have to compare their polarizabilities α where the magnitude of the α_{zz} component would be the most important. Since this is not the case, we consider here only the fact that both reactants "communicate" via their polarizing power and their polarizability. Polarization of the charge distribution of acetylene leads to an induced dipole moment, which in turn polarizes the charge distribution of the 1,3-dipole molecule. The latter process depends on its polarizability where again the zz-component of the polarizability tensor rather than the isotropic polarizability will be important. A large α_{zz} facilitates the reaction and leads to a lower reaction barrier.
4. The fourth property, which strongly influences reaction rate and reaction mechanism, is the ability of both partners of accepting or donating charge. Previous studies have discussed the charge transfer between dipolarophile and 1,3 dipole within the framework of the frontier molecular orbital (FMO) theory. Using this concept, the 1,3-dipoles were categorized as being nucleophilic [Nucl(HOMO); Fig. 1] donating charge from their HOMO to the LUMO of the dipolarophile, electrophilic [Elec(LUMO); Fig. 1] accepting charge from the dipolarophile in their LUMO, or amphiphilic [Amphi(HOLU), Fig. 1] reacting either way depending on the character of the dipolarophile [1–5]. We have investigated the charge transfer between the reactants and found, contrary to the qualitative description of FMO theory, that the charge transfer starts already in the van der Waals region, i.e., in phase 1. Then, it is directed from the 1,3-dipole to the acetylene molecule and continues to develop to its full strength in phase 2 (compared with Fig. 4a and b).

On the basis of these facts, the curvature of the reaction path, and its decomposition into local mode curvature coupling coefficients (see Fig. 2a–j), one can describe the events in phase 1 as follows where system **4** (Fig. 2d) is used as an example. Guided by the form of its exchange repulsion envelope, HCNO approaches acetylene as much as possible at its O terminus (Z4), which leads to an inclination angle of 41°. Accordingly, the local mode curvature coupling coefficients associated with the orientation angles C3C1O4 and C1C3C2 become relatively

Table 2 Properties of 1,3-dipoles and reaction complexes **1–10**: Dipole moment component μ_z and total dipole moment μ_{total} (in parenthesis), polarizability component α_{zz} and isotropic polarizability α_{iso} (in parenthesis) of the reaction complex calculated for the complex geometry at the first point of the reaction path in the entrance channel

System	μ_z (μ_{total}) [Debye]	α_{zz} (α_{iso}) (Å^3)	k^a(XYZ) (mdyn Å/rad^2)	ω^a(XYZ) (cm^{-1})	ω_μ(XYZ) (cm^{-1})	k^a(C3X2) (mdyn/Å)	k^a(C1Z4) (mdyn/Å)	ω_μ(C3X2) (cm^{-1})	ω_μ(C1Z4) (cm^{-1})	Orientation (°)	Charge pol. (me)	Δ s(TS) [amu$^{1/2}$ Bohr]
1 (NNO)	−0.01 (0.01)	4.1 (2.1)	0.693	604	604 (599)	5.506	5.766	1,113	1,166	5.4	8	4.1
2 (NNNH)	1.03 (1.95)	5.4 (2.8)	0.618	563	530 (520)	5.853	6.802	1,185	1,469	0.9	−23	5.0
3 ($NNCH_2$)	1.69 (1.72)	6.3 (3.4)	0.600	549	590 (582)	3.959	4.509	964	992	−10.3	−14	4.4
4 (HCNO)	−2.43 (3.16)	3.7 (2.7)	0.513	517	569 (565)	5.789	5.879	1,051	1,132	41.2	55	5.5
5 (HCNNH)	−0.20 (2.08)	6.5 (3.7)	0.598	546	535 (531)	6.039	6.838	1,064	1,153	21.0	22	6.3
6 ($HCNCH_2$)	0.74 (1.66)	8.3 (4.5)	0.605	544	494 (492)	4.222	4.699	936	1,011	−18.0	−47	5.7
7 (H_2CNHO)	−2.85 (3.44)	5.2 (3.4)	1.490	761	572 (570)	4.121	5.130	943	1,072	17.1	103	4.3
8 (H_2CNHNH)	−1.60 (2.37)	4.9 (4.1)	1.417	744	544 (545)	4.092	4.534	946	1,095	36.5	38	4.8
9 (H_2CNHCH_2)	0.00 (1.36)	9.0 (5.0)	1.173	675	477 (479)	3.941	3.941	967	967	0	0	5.5
10 (ONHO)	0.00 (2.59)	3.5 (2.2)	2.061	914	783 (782)	4.535	4.535	976	976	0	0	5.0

Direction z is defined by the acetylene CC axis. Local mode force constant $k^a(XYZ)$, local mode frequency $\omega^a(XYZ)$, and normal mode bending frequency $\omega_\mu(XYZ)$ of the isolated 1,3-dipole molecule (values in parentheses correspond to normal mode XYZ bending frequencies of the reaction complex calculated for the complex geometry at the first point of the reaction path in the entrance channel); local mode force constants $k^a(C3X2)$ and $k^a(C1Z4)$, normal mode frequencies $\omega_\mu(C3X2)$ and $\omega_\mu(C1Z4)$ of the product; orientation angle of the 1,3-dipole (X2Z4 axis) relative to the CC axis of acetylene and charge polarization in acetylene (surplus of negative charge at C1H compared to HC3) calculated for the complex geometry at the first point of the reaction path in the entrance channel; shift parameter $\Delta s(TS)$ of the TS relative to the center M3 of bond formation

large and they are responsible (via their squares) for a significant curvature enhancement in phase 1. Since in this phase, C1Z4 and C3X2 are approach parameters measuring the degree of exchange repulsion, their curvature coupling coefficients can also make a contribution to the scalar curvature; however, they will always be negative, i.e., the reaction complex resists a shortening of the approach distance (a closer approach requires energy).

Because of a substantial magnitude of the μ_z-component (−2.43 D), the charge of acetylene is polarized so that the C3H end becomes negative and the C1H end positive (difference in local charges 55 me). At the same time as charge polarization starts, also the charge transfer to acetylene begins (see Fig. 4b). Hence, phase 1 can be characterized as the orientation, polarization, and charge transfer phase, in which the electronic structure of the reactants is not significantly altered. In this sense, one can also speak of a van der Waals phase. Phase 1 will be well developed in the curvature diagram if the orientation of the reactants to each other is important as reflected by the orientation angle of Table 2. Reaction systems **1**, **2**, and **9** have small or zero orientation angles, and therefore, phase 1 is rather small (see Fig. 2a, b, i).

Reaction Phase 2 (from curvature point M1 to curvature point M2): As Fig. 4b reveals, charge transfer fully develops in phase 2, which we call the rehybridization phase as will be explained below. Charge transfer to acetylene and the simultaneous polarization of the acetylene density leads to a labilization that invokes bending and the formation of a radicaloid center. If acetylene accepts negative charge, it will try to adopt a bent structure. The amount of bending at each terminus depends on whether the charge is equally distributed in the corresponding $\pi^\star$ MO (see **9**) or, via charge polarization, shifted to the CH group farther away from the more electronegative terminal group of the 1,3-dipole. When free acetylene accepts negative charge, a trans form is adopted, which is also formed in phase 1 (supported by attraction with an electronegative terminal group Z4 (X2)), however with bending angles deviating by just a couple of degree from the linear form (revealed by the local mode curvature coupling coefficient of the HCC bending type in phase 1). In phase 2, however, acetylene is forced into a cis-bended form (e.g., **9**) or a form significantly bent at just one center whereas the other CCH unit remains quasi-linear.

We have investigated the local vibrational modes of a charge-polarized acetylene molecule and find a smaller bending force constant for the more negatively charged acetylene terminus. Hence, charge transfer and charge polarization are the driving forces for bending and rehybridization of acetylene. A radicaloid or biradicaloid center(s) with fractional unpaired electrons protruding in the direction of the attacking 1,3-dipole is (are) generated. The

HCC local mode curvature coupling coefficients clarify which HC group bends first. In all those cases where an electronegative group in the 1,3-dipole leads to a larger orientation angle, the not directly attacked CCH group bends more and becomes the location for the first bond formation. This means that a close attack on one CH terminus of acetylene causes the other terminus to prepare first for bonding.

Charge loss leads to a labilization of the rigid (multiple) bond structure of the 1,3-dipole so that bending becomes possible. The curvature enhancement in phase 2 is dominated by the XYZ and CCH local mode curvature coupling coefficients. These are negative, thus indicating that energy is required to enforce rehybridization and bending of the two reactants. Both reactants change at the same time so that there is no way of saying that the one or the other reactant is leading the reaction. However, snapshots of the geometry and the curvature coupling coefficients reveal that in asymmetric cases with a sizable orientation angle, bending of one HCC acetylene group is clearly ahead of the other CCH group.

The charge transfer curves shown in Fig. 4b reveal that there is a clear distinction between the 1,3-dipole molecules with regard to charge-donating capacities. This is large for nucleophilic 1,3-dipoles (see Fig. 1) and extends beyond the TS, thus leading to relatively low energy barriers (compared to all other cycloaddition systems or within a given group as, e.g., in the group of the diazonium betaines in the case of reaction system **3**). For electrophilic 1,3-dipoles such as **1**, the labilization of acetylene is not sufficient for the formation of a radicaloid center and therefore a large energy barrier results (Table 1). For the purpose of verifying this hypothesis, we investigated also the cycloaddition of the strongly electrophilic 1,3-dipole molecule nitryl hydride to acetylene (system **10**, Fig. 2j) and found the predicted reaction behavior: Insufficient charge transfer (see Fig. 4b) is coupled with a relatively large reaction barrier of 29.4 kcal/mol (Table 2).

In view of the nature of the curvature enhancement dominating reaction phase 2, we speak of the rehybridization and bending phase, which leads to the formation of (bi)radicaloid centers.

Reaction Phase 3 (from curvature point M2 to curvature point M3): Reaction phase 3 can be distinguished from phase 4 only in the case of reaction systems **3**, **4**, and **5** where a curvature peak of medium size results from the formation of the first bond between the reactants. In all other cases, the scalar curvature of phase 3 appears as a shoulder of a large curvature peak developing in phase 4. Nevertheless, a distinction between phases 3 and 4 becomes possible when one investigates the local mode curvature coupling coefficients of the two bond formation processes. In phase 3, one is positive (bond formation supporting) and the other negative (bond formation resisting). Therefore, it is justified to characterize phases 3 and 4 as the first and second bond formation phases.

In phase 3, the C3X2 bond curvature coupling coefficient is positive (when Z4 corresponds to the electronegative terminus of the 1,3-dipole), whereas the C1Z4 interaction (characterized by a negative curvature coupling coefficient) is still resisting bond formation. This corresponds to the fact that bond C3X2 is formed before bond C1Z4. In phase 1, the electronegative end of the 1,3-dipole is much closer to acetylene, suggesting that bond C1Z4 is formed first. However, charge transfer and charge polarization facilitate the formation of a radicaloid center at the other terminus. Radicaloid centers with lower exchange repulsion between them can bridge much easier a larger distance so that bond formation, contrary to general expectations, takes place earlier between the atoms farther apart.

In the cases of systems **2** and **3** (N2 is now the electronegative end), the situation is reversed and the C1Z4 curvature coupling coefficient is ahead of the resisting C3X2 curvature coupling coefficient, indicating that the C1Z4 bond is formed now before the C3X2 bond. In case of symmetry, phase 3 is less pronounced and is dominated by C1C3 and C2N5C4 adjustments. This is also true for system **6** for which both termini of the 1,3-dipole have similar electronegativities.

Reaction Phase 4 (from curvature point M3 to the end in exit channel): The question, which bond is formed first when generating the five-membered ring, can be easily answered by inspection of the components dominating the reaction path direction. Reaction path direction and reaction path curvature are complementary in so far as a local mode, when making a large contribution to one of the path quantities, can only make a small contribution to the other. As shown in Fig. 3 for the reaction path direction of system **4** (HCNO), the approach distances C2C3 and C1O4 dominate the path direction for most of its range. The amplitude of the mode associated with parameter C2C3 drops to small values between s = 3 and s = 5 amu$^{1/2}$ Bohr in phase 3, which is exactly that location where the C2C3 bond is formed. A similar decrease in the amplitude of the mode associated with C1O4 occurs much later in phase 4 when the C1O4 bond is finalized. Hence, the formation of the five-membered ring bonds is asynchronous with the less polar bond C2C3 being formed first in phase 3 (when C1O4 is still resisting bond formation) and the more polar bond C1O4 later in phase 4.

The less polar bond in **4** is formed by electron pairing in a *soft*, homolytic fashion leading to a smaller curvature enhancement or just a shoulder. For the formation of the more polar bond, exchange repulsion has to be overcome and a stronger bond is formed. This leads to a large

curvature peak, which is enhanced by contributions from the adjustment steps of the other bonds in the five-membered ring being formed. In the case of the symmetric systems **9** and **10**, the simultaneous formation of the two new bonds leads to a large curvature.

The delay between the formation of X2C3 and C1Z4 is proportional to the electronegativity difference between termini X and Z. The new bonds are formed at the same time for systems **9** and **10** (because of symmetry). In the case of systems **2** and **6**, formation takes place almost at the same time because the electronegativities of groups N and NH or HC and CH_2 are almost the same.

There is a basic difference between reaction systems **1**–**6** and systems **7**–**9** because in the former cases a planar five-membered ring is formed characterized by electron delocalization, i.e., the new bonds adopt some double-bond characters whereas in the latter cases puckered rings are generated with little electron delocalization and the new bonds being essentially single bonds. Although the degree of puckering is small (puckering amplitudes [87–89] q are 0.187 (**7**), 0.098 (**8**), and 0.146 Å (**9**), which correspond to maximal dihedral angles of 19.0, 9.9, and 14.7°, respectively), it leads to unique ring conformations (a twist form close to pseudorotation phase angle [87–89] $\phi = 342°$ for **7**, an envelope form close to $\phi = 324°$ for **8**, and a pure envelope form with an axial NH bond with $\phi = 180°$ for **9**; see bottom of Fig. 1), which are optimal with regard to anomeric stabilization and bond staggering.

When these single bonds are finalized, the five-membered ring adjusts to its equilibrium conformation. This adjustment does not require significant electronic structure changes, and therefore, the curvature is small in the last part of phase 4 of the corresponding cycloaddition reactions (see Fig. 2g–i). In the other six systems (including also system **10**), the last stage of phase 4 corresponds to π-delocalization, which is connected with a relatively large curvature. This is also relevant for the reverse reaction: The splitting of the two bonds requires initially major electron reorganization, and the scalar curvature starts with a high value.

Discussion of the reaction energetics The discussion of the reaction mechanism of cycloaddition systems **1**–**9** reveals a close mechanistic relationship, which should make it possible to explain the energetics of these reactions in a consistent way. Clearly, the fate of the reaction complex with regard to stereochemistry or the sequence of the bond formation steps is early decided in phase 1 (van der Waals phase). Orientation of the reactants, charge transfer to acetylene, and mutual polarization in phase 1, although decisive, involve only minor energy changes. The major changes in the electronic structure of the reactants occur in phase 2 (rehybridization and bending phase), in which via bending of the XYZ-dipole molecule, the pyramidalization of the terminal $-CH_2$ groups (if existent), and bending of one or both CCH units of acetylene, the radicaloid centers are prepared so that bond formation becomes possible.

In all cases investigated, the TS is located in phase 2 always before (or at) the end of this phase given by M2 and thereby always after the curvature peak. Since at this curvature peak the largest change in energy takes place (strongest change in the electronic structure) in the entrance channel, it is reasonable to assume that the energy difference $\Delta E(P2) = E(M2) - E(M1)$ must be proportional to the activation energy. This hypothesis is confirmed by Fig. 5 where calculated $\Delta E(P2)$ values are correlated with the energy barriers. The energy changes in phase 2 determine the reaction barrier; however, this does not say that they determine the mechanistic sequence, which obviously is determined already in phase 1.

There are three electronic factors determining the barrier.

1. The reaction barriers decrease linearly with (absolutely seen) increasing dipole moment μ_z (parallel to the CC axis of acetylene, see Table 2) where the correlation is more significant with the more accurate CCSD(T)-F12 barriers. The polarizing power of the 1,3-dipole expressed in this way has a larger effect for the more electrophilic dipoles **1**, **2**, and **3** than for the more nucleophilic dipoles **7**, **8**, and **9**.
2. The reaction barriers also decrease with increasing polarizability component α_{zz} (see Table 2). This effect is best developed for the 1,3-dipoles with linear XYZ unit (**1**–**6**) and less for the bent dipoles (the azomethines, see Fig. 1) with a three-dimensional structure. The larger the polarizability component α_{zz} is, the easier can be the density of the 1,3-dipole molecule polarized so that radicaloid centers are formed.
3. Also shown in Table 2 are the local mode XYZ bending force constants k^a, which are a measure for the ease of bending of the heavy atom framework of XYZ in phase 2. For the diazonium betaines and the azomethines investigated, a larger bending force constant (in line with a larger electronegativity difference between X and Z) leads to a larger barrier. This effect is, however, outweighed by the charge polarization and polarizability effects in the case of the nitrilium betaines.

In Table 2, the calculated local mode stretching force constants k^a of bonds C3X2 and C1Z4 of the newly formed five-membered rings are also given. They confirm that the more polar bond (formed after the less polar bond) is always the somewhat stronger (corresponding to a larger k^a value). The sum of these k^a values reflects whether a planar

ring with a delocalized 6π-system is formed (large sum) or a (non)planar ring with limited π-delocalization. In the former case, the barrier for cycloreversion is high.

Differences between the various cycloaddition reactions Although the reaction mechanisms of the ten cycloadditions investigated in this work are very similar, there are also remarkable differences, which become apparent from the URVA analysis.

1. Differences between the reaction of an electrophilic and a nucleophilic 1,3-dipole (for the former the charge transfer ceases already in the entrance channel, whereas for the latter it has it maximum in the exit channel);
2. Differences between symmetric and asymmetric 1,3-dipoles (for the former, phase 3 is a phase to prepare the reaction complex for bond formation, whereas for all other reaction systems, phase 3 is the phase for forming the soft bond via long-range interactions between radicaloid centers);
3. Similarly, there is a difference between 1,3-dipoles with termini of similar or strongly different electronegativities;
4. Diazonium and nitrilium betaine reactions lead to a different phase 4 compared to that of the azomethine cycloadditions (the product of the former reactions is a planar ring with electron delocalization, and therefore, phase 4 encompasses this process indicated by a large scalar curvature at the end of the phase. The latter reaction systems lead to a puckered ring, and therefore, phase 4 is characterized by a small curvature peak and small curvature values at the end reflecting a conformational adjustment);
5. If the orientation phase includes conformational adjustments of the 1,3-dipole, it is characterized by a larger curvature enhancement. Such a case is given by system **5** where the orientation leads to a rotational adjustment of the 1,3-dipole in the reaction complex (see Fig. 2e);
6. There is a fine distinction between different reaction systems depending on whether the trans-bending mode of acetylene is strongly, just weakly, or not at all excited in the entrance channel so that the radicaloid centers of acetylene develop with a very different pace (see below);
7. Systems such as **6** and **8**, which possess identical reaction barriers within calculational accuracy, have different reaction mechanisms as can be seen from the curvature diagrams in phase 4 (see Fig. 2f, h). This reflects that the TS and energy barrier are just cumulative descriptors of a reaction, which result from different electronic effects and their changes, but which do not provide a detailed insight into the mechanism.

Comparison with other mechanistic studies In the "Introduction," three mechanistic hypotheses are mentioned, which are currently used to explain mechanistic details of 1,3-dipolar cycloaddition reactions. They are discussed below.

The distortion energy description Houk et al. [30, 32] introduced the *distortion energy* as the energy required to distort the dipole and the dipolarophile into the TS geometries without allowing any interaction between them. The total activation energy is the sum of the distortion and interaction energy of the two distorted fragments frozen in the TS geometry. These authors found a strong correlation between the activation energy and the distortion energy for the reaction of dipoles **1**–**9** with ethylene and acetylene. Based on these findings, they concluded that the concerted mechanism leads to a TS geometry at which the overlap between the orbitals of the termini of the cycloaddends directly leads to the cycloadduct without further geometry distortion. To achieve this, the TS geometry requires distortion of the dipole, and the distortion is related to the dipole stability.

These observations are in line with the URVA results in so far as the TSs of the 1,3-dipolar cycloadditions are located close to the end of the rehybridization phase, which is the phase with the energy-consuming electronic structure changes. In many other cases investigated so far, the TS occurs at a less prominent position, which would make the mechanistic interpretation of the distortion energy more difficult [53, 65–67, 90].

Conventional investigations of chemical reactions focus on the explanation of the height of the reaction barrier. This is important, however, that the reaction barrier alone cannot provide a detailed insight into the reaction mechanism as presented in this work. As shown above, similar reaction barriers do present neither a necessary nor sufficient condition for similarity of the reaction mechanism. Likewise, two reactions may have similar mechanisms although they have different barriers. The energy barrier of a reaction is just a cumulative measure of all electronic structure changes taking place at the position of the TS, and therefore, it can only provide indirect and remote insight into the electronic structure changes taking place during the reaction.

The bending hypothesis Houk and coworkers concluded that the correlation of the activation energy with the distortion energy implies that the vibrational excitation of the reactants is an important feature of the mechanism [28]. When analyzing the transition vector for the reactions of the diazonium betaines **1**–**3** with acetylene or ethylene, these authors found that the translational vector associated with the imaginary frequency is dominated by the bending of the 1,3-dipole (up to 80 %). Classical trajectory calculations confirmed the dominance of the dipole bending

excitation, which parallels the trend in the distortion energies. Barnes and Hase performed variational transition state calculations for the cycloaddition of diazonium betaines **1**–**3** and ethylene [14]. They concluded that the reaction rate for a fixed temperature will be increased by selective excitation of the diazonium betaines bending vibrational modes in line with Houk's findings.

The analysis of the reaction path direction reveals that in none of the reaction systems investigated does bending dominate the path direction. However, the curvature enhancements shown in phase 2 are dominated by the normal mode curvature coupling coefficient associated with the XYZ and acetylene bending modes. Hence, pumping up these modes will lead to an acceleration of the reaction, provided the energy channeled into the bending modes is not dissipated by Coriolis couplings with other vibrational modes.

In Fig. 7a, the normal mode frequencies of reaction complex **4** are given as a function of the reaction parameter s in the range up to 1200 cm^{-1}, which includes all bending and torsional modes. Also shown are the avoided crossings (ACs) between vibrational states of the same symmetry AC1 to AC14, which are the positions of strong mode–mode couplings. Clearly, there is the possibility of a continuous exchange of energy between the vibrational modes along the reaction path, which should lead to energy dissipation and thereby a reduction in mode-selective rate enhancement.

If energy dissipation, involving key vibrational modes, takes place before the TS, mode-selective rate enhancement is quenched. Figure 7a and b shows that in the entrance channel the XYZ bending mode, # 7, undergoes Coriolis coupling with the trans-HCCH bending mode, # 9, at $s = -6.85$ $amu^{1/2}$ Bohr (AC1) and at $s = -1.80$ $amu^{1/2}$ Bohr (AC4), which leads to a mixing of their characters and an exchange of energy. Shortly before the TS, there is another avoided crossing (AC5) involving modes #7 and #10. This will effectively dissipate any energy pumped into the XYZ bending mode # 7, which is in contrast to the hypothesis of Houk [28] and Hase et al. [14].

The analysis of normal modes #7, #9, and #10 reveals that energy stored in the first two modes can be transferred to the cis-bending mode of HCCH (see Fig. 7a, b). This mode must be triggered to establish radical centers at C1 and/or C3. Any energy stored in the XYZ bending mode #7 will activate cis-HCCH bending, which may accelerate the reaction as long as XYZ bending takes place at the same time. However, this cannot be guaranteed on the basis of the mode–mode coupling situation before the TS.

All ten reaction systems investigated exhibit a similar mode–mode coupling pattern, which leads to an energy dissipation between those bending modes, which must be excited for rate acceleration. Hence, the previous observations of Houk and Hase are confirmed even though complicated Coriolis coupling patterns as shown in Fig. 7a normally make mode-selective rate enhancements ineffective. It will be interesting to see whether other dipolarophiles than acetylene lead to the same effective mechanism despite a multitude of dissipation possibilities.

The biradical hypothesis Hiberty et al. [12] found a correlation between the biradical character of 1,3-dipoles **1-9** and their reactivity toward ethylene or acetylene using the breathing-orbital valence bond ab initio method [20]. Each 1,3-dipole is described as a linear combination of three valence bond structures, two zwitterions and one biradical, for which the weights in the total wave function can be quantitatively estimated.

A reaction mechanism was proposed [12], in which the 1,3-dipole first distorts so as to reach a reactive electronic state that has a significant biradical character, which then adds with little or no barrier to the dipolarophile. By determining the biradical character of the 1,3-dipole either as the weight of the biradical structure at equilibrium or as the energy gap between the ground state of the 1,3-dipole and its biradical diabatic state, they found a useful correlation between the biradical character and the barrier heights. In line with Houk′s energy distortion/interaction model, the barrier height for the cycloaddition of a given 1,3-dipole to ethylene or acetylene is dominated by biradical energy, which rationalizes that for both ethylene and acetylene addition, the barrier heights are nearly the same despite significant differences in the exothermicity of these reactions.

Again, this approach provides an energy-counting argument, which does not necessarily lead to a mechanistic insight. As shown in this work, the reaction is initiated by a charge transfer to the dipolarophile and polarization of the density of the latter. The generation of (a) (bi)radicaloid center(s) at acetylene is as important as that at the 1,3-dipole molecule and precedes or is parallel to the bending of the 1,3-dipole. Also as noted above the major part of the reaction barrier is due to the rehybridization and (bi)radicaloid formation of the 1,3-dipole. However, mechanistically more important are the charge transfer, the population of a $\pi^{\star}$(HCCH) orbital, and the *softening* of the bending motion, which is the prerequisite for radicaloid formation. In the first phase, the 1,3-dipole polarizes the acetylene molecule and not vice versa. The difference in electronegativities of the 1,3-dipole termini X and Z decides on the amount of charge transfer and the polarization.

We can distinguish between 1,3-dipolar cycloadditions, which start with just one radicaloid center (bending of one CCH group: e.g., system **4**) and those which, because of symmetry or similar electronegativities of X and Z, require the bending of both CCH groups in acetylene and the formation of a biradicaloid (e.g., systems **9** or **6**). This

mechanistic differentiation is supported by a sophisticated energy exchange between 1,3-dipole bending, HCCH trans-bending, and HCCH cis-bending motions before the TS. In view of the URVA analysis presented in this work, it is appropriate to speak in this connection of radicaloid- and biradicaloid-driven cycloadditions. However, it would be a simplification to consider just the biradical formation of the 1,3-dipole molecule excluding the role of the dipolarophile.

The Hammond–Leffler postulate The Hammond–Leffler postulate, although not directly formulated in this way [91, 92], derives from the exothermic or endothermic character of a reaction a characterization of the TS as being early (in the first case) and late (in the second case). A quantification of this postulate has turned out to be difficult until recently. We showed that the TS of a reaction is shifted against the center of the bond-breaking/forming processes (identified via scalar curvature and local mode curvature coupling coefficients) by an amount $\Delta s(TS)$ along the reaction path, which is proportional to the reaction energy, $\Delta_R E$ [69, 93]. The larger the shift parameter is, the more exothermic the reaction is, and the earlier the TS is located in the entrance channel. For endothermic reactions, the shift parameter becomes negative [69, 93].

In Fig. 6, the $\Delta s(TS)$ values obtained in this work (see also Table 2) are given in dependence of the calculated reaction energies $\Delta_R E$. A linear relationship results, which identifies reaction systems **5**, **6**, **4,** and **9** as having an early TS. This is a result of forming a stable five-membered ring (a pyrazole, isoazole, or isoxazole with a delocalized 6π-electron system) or converting an unstable 1,3-dipole such as the azomethine ylide of reaction system **9** with high biradical character into a more stable 2,5-dihydro-pyrrole. The scalar curvature presents an important tool to verify and quantify the Hammond–Leffler postulate.

4 Conclusions

This investigation confirms that chemical reactivity is the result of the mutual polarization of the reactants (proportional to their polarizing power and polarizability) and charge transfer between them, which leads to a change in their electronic structure and prepares them for the reaction.

1. All ten 1,3-dipolar cycloadditions investigated in this work with URVA follow a 4-phase reaction mechanism with well-defined reaction phases defined by the scalar curvature of the reaction path and features of the unified reaction valley. These phases are identified and characterized in their chemical nature with the help of the local mode curvature coupling coefficients.
   (1) *Reaction phase 1* is the orientation phase where charge transfer and charge polarization are initiated;
   (2) *Reaction phase 2* is the rehybridization and bending phase where radicaloid or biradicaloid structures are formed;
   (3) *Reaction phase 3* is the phase where the homolytic formation of the *softer* bond starts;
   (4) In *Reaction phase 4* being characterized by a large curvature peak, the formation of the *harder* (more polar) bond and the finalization of the new five-membered ring take place, accompanied by π-delocalization (systems **1**–**6** and **10**) or ring puckering (systems **7**–**9**).
2. The orientation of the 1,3-dipole XYZ relative to acetylene is a consequence of the shape of the exchange repulsion envelope around the 1,3-dipole. This in turn depends on the electronegativity difference between X and Z. The orientation of the 1,3-dipole determines the degree of charge transfer and charge polarization and decides on the asynchronicity of the formation of the two five-membered ring bonds. Hence, the mechanism of the cycloaddition reaction is decided early in the van der Waals range (phase 1). It is important to note that *the bond with larger CX or CZ distance in the orientation phase is formed first*, which has to do with the fact that two radical centers can undergo long-range interactions.
3. The driving force of all ten cycloaddition reactions is the charge transfer from the 1,3-dipole to the acetylene molecule. This is also true for the electrophilic 1,3-dipole molecules, which differ from the nucleophilic dipoles by a reduced charge transfer ability ceasing before the TS (see Fig. 4b). Consequently, a much higher energy barrier results. The amount of charge transfer can be qualitatively predicted by investigating the frontier orbitals of 1,3-dipole and dipolarophile, which explains the success of FMO theory for describing these types of reactions. However, we also note that the detailed information provided by the URVA analysis of a reaction (see, e.g., Fig. 4b) cannot be expected from FMO theory.
4. In separate calculations, we have shown that any transfer of negative charge into the $\pi^\star$ MO of acetylene leads to trans-bending, which is initiated in phase 1, although it is in conflict with the actual cis-bending required later in the reaction. Charge polarization in acetylene as induced by the approaching 1,3-dipole triggers CCH bending at the more negatively charged acetylene terminus as could be shown with the help of the local mode bending force constants.

5. The 1,3-dipolar cycloaddition reactions are the first reactions investigated so far [55, 65–69, 74, 90] for which the mechanistically important electronic structure changes take place in the phase (here phase 2) containing the TS so that the reaction barrier is almost identical to the energy changes in this phase (phase 2; see Fig. 5). In most other reactions, the location of the TS is not significant for the individual mechanistic changes because it is just an *accountant* for the sum of all energy changes rather than a descriptor of specific energy changes associated with individual mechanistic steps.
6. The energy barrier is determined by mutual charge polarization of the reactants and therefore directly related to the polarizing power and the polarizability of the 1,3-dipole molecule as reflected by its dipole moment component in the direction of the acetylene molecule and its polarizability component in the same direction.
7. Another factor influencing the magnitude of the reaction barrier is the stiffness of the XYZ-dipole as measured by the local XYZ bending force constant. A large (small) force constant implies a large (small) barrier apart from the nitrilium betaines where mutual polarization effects dominate the reaction barrier. The local stretching force constants of the five-membered rings formed reflect their degree of electron delocalization and they are measures for the height of the barrier of the cycloreversion reaction.
8. Previous work emphasizing the importance of an excitation of the XYZ bending vibration for a mode-specific acceleration of the reaction is confirmed, however, with some important restrictions. There is a multitude of Coriolis couplings, which in general dissipate any mode-specific energy surplus. In the case of the cycloaddition reactions **1**–**10**, the peculiar situation exists that XYZ bending couples with trans- and cis-bending of HCCH in the entrance channel so that any energy excess in the XYZ bending mode facilitates the formation of radicaloid centers in the dipolarophile without guaranteeing that XYZ bending is enhanced. Future investigations have to clarify whether this is a more general phenomenon.
9. The center of the chemical processes of bond forming leading to the five-membered ring is located in the exit channel. The shift parameter $\Delta s(TS)$ measures the earliness of the TS according to the Hammond–Leffler postulate and correlates linearly with the exothermicity of the reaction as described by $\Delta_R E$, thus providing a quantitative confirmation of this postulate.

The chemical reaction mechanism of the 1,3-dipolar cycloadditions is determined in the van der Waals range far off the TS. It is typical of a symmetry-allowed pericyclic reaction that the energy needed to overcome the reaction barrier is used to *prepare* the reactants for the reaction and that the actual bond formation takes place after the TS in the exit channel. The stability of the bonds being formed and the degree of electron delocalization in the five-membered ring determine the exothermicity of the reaction.

The many mechanistic details, which the URVA analysis of the 1,3-dipolar cycloadditions unravels, provide a solid basis for predictions concerning changes in the reaction mechanism and the energetics upon replacing the dipolarophile, substituting 1,3-dipole and/or dipolarophile, or using metal catalysis to accelerate the cycloaddition reaction. Any means that (1) increase the charge transfer to the dipolarophile and/or (2) facilitate its charge polarization will lower the barrier of the cycloaddition. Substituents of the 1,3-dipole will lower the barrier if they increase its polarizability and charge polarization in such a way that the asynchronicity of bond formation is supported rather than hindered. The same applies also with regard to steric effects. In view of the lengths of this work, the detailed discussion of these effects will be the topic of a forthcoming publication.

Acknowledgments This work was financially supported by the National Science Foundation, Grant CHE 1152357. We thank SMU for providing computational resources.

References

1. Padwa A, Pearson WH (2002) Synthetic applications of 1,3-dipolar cycloaddition chemistry toward heterocycles and natural products. Wiley, New York
2. Nair V, Suja TD (2007) Intramolecular 1,3-dipolar cycloaddition reactions in targeted syntheses. Tetrahedron 63:12247–12275
3. Padwa A, Bur SK (2007) The domino way to heterocycles. Tetrahedron 63:5341–5378
4. Rane D, Sibi M (2011) Recent advances in nitrile oxide cycloadditions. Synthesis of isoxazolines. Curr Org Synth 8:616–627
5. Kaur J (2011) Azomethines and 1,3 dipoles—leading to new heterocycles: studies on 1,3 dipolar cycloadditions. LAP LAMBERT Academic Publishing, New York
6. Woodward RB, Hoffmann R (1969) The conservation of orbital symmetry. Angew Chem Int Ed Engl 8:781–853
7. Dewar MJS (1971) Aromaticity and pericyclic reactions. Angew Chem Int Ed Engl 10:761–776
8. Nguyen TA (2007) Frontier orbitals: a practical manual. Wiley, New York
9. Gold B, Dudley GB, Alabugin IV (2013) Moderating strain without sacrificing reactivity: design of fast and tunable noncatalyzed alkyne-azide cycloadditions via stereoelectronically controlled transition state stabilization. J Am Chem Soc 135:1558–1569
10. Barbosa AGH, Monteiro JGS (2012) On the electronic structure of the diazomethane molecule. Theor Chem Acc 131:1297–1323
11. Das TK, Salampuria S, Banerjee M (2010) Computational DFT study of the 1,3-dipolar cycloadditions of 1-phenylethyl- trans-2-

methyl nitrone to styrene and 1-phenylethyl nitrone to allyl alcohol. J Mol Struc Theochem 959:22–29
12. Braida B, Walter C, Engels B, Hiberty PC (2010) A clear correlation between the diradical character of 1,3-dipoles and their reactivity toward ethylene or acetylene. J. Am. Chem. Soc. 132:7631–7637
13. Engels B, Marian CM (2009) What controls the reactivity of 1,3-dipolar cycloadditions? Angew Chem Int Ed Engl 48:7968–7970
14. Barnes GL, Hase WL (2009) Bent out of shape. Nat Chem 1:103–104
15. Mladenovic M, Elhiyani M, Lewerenz M (2009) Electric and magnetic properties of the four most stable CHNO isomers from ab initio CCSD(T) studies. J Chem Phys 131:034302–1–034302–14
16. Mladenovic M, Lewerenz M, McCarthy MC, Thaddeus P (2009) Isofulminic acid, HONC: ab initio theory and microwave spectroscopy. J Chem Phys 131:174308–117430810
17. Benchouk W, Mekelleche SM (2008) Theoretical analysis of the regioselectivity of 1,3-dipolar cycloaddition of C-(methoxycarbonyl)-N-methyl with methyl acrylate and vinyl acetate. J Mol Struc Theochem 852:46–53
18. Merino P, Tejero T, Chiacchio U, Romeoc G, Rescifina A (2007) A DFT study on the 1,3-dipolar cycloaddition reactions of C-(hetaryl) nitrones with methyl acrylate and vinyl acetate. Tetrahedron 63:1448–1458
19. Sakai S, Nguyen MT (2004) Theoretical determination of the electronic mechanisms of 1,3-dipolar cycloaddition reactions of fulminic acid and diazomethane. J Phys Chem A 108:9169–9179
20. Hiberty PC, Shaik S (2002) A clear correlation between the diradical character of 1,3-dipoles and their reactivity toward ethylene or acetylene. Theor Chem Acc 108:255–272
21. Nguyen MT, Chandra AK, Sakai S, Morokuma K (1999) Another look at the mechanism of the concerted 1,3-dipolar cycloaddition of fulminic acid to acetylene. J Org Chem 64:65–69
22. Lopez SA, Munk ME, Houk KN (2013) Mechanisms and transition states of 1,3-dipolar cycloadditions of phenyl azide with enamines: a computational analysis. J Org Chem 78:1576–1582
23. Lan Y, Wheeler SE, Houk KN (2012) Extraordinary difference in reactivity of ozone (OOO) and sulfur dioxide (OSO): a theoretical study. J Chem Theory Comput 7:2104–2111
24. Krenske EH, Houk KN, Holmes AB, Thompson J (2011) Entropy versus tether strain effects on rates of intramolecular 1,3-dipolar cycloadditions of N-alkenylnitrones. Tetrahedron Lett 52:2181–2184
25. Lan Y, Houk KN (2010) Mechanism and stereoselectivity of the stepwise 1,3-dipolar cycloadditions between a thiocarbonyl ylide and electron-deficient dipolarophiles: a computational investigation. J Am Chem Soc 132:17921–17927
26. Xu CE, Doubleday L, Houk KN (2010) Dynamics of 1,3-dipolar cycloadditions: energy partitioning of reactants and quantitation of synchronicity. J Am Chem Soc 132:3029–3037
27. Xu CE, Doubleday L, Houk KN (2009) Dynamics of 1,3-dipolar cycloaddition reactions of diazonium betaines to acetylene and ethylene: bending vibrations facilitate reaction. Angew Chem Int Engl 48:2746–2748
28. Schoenebeck F, Ess DH, Jones GO, Houk KN (2009) Reactivity and regioselectivity in 1,3-dipolar cycloadditions of azides to strained alkynes and alkenes: a computational study. J Am Chem Soc 131:8121–8133
29. Ess DH, Jones GO, Houk NK (2008) Transition states of strain-promoted metal-free click chemistry: 1,3-dipolar cycloadditions of phenyl azide and cyclooctynes. Org Lett 10:1633–1636
30. Ess DH, Houk KN (2008) Theory of 1,3-dipolar cycloadditions—distortion/interaction and frontier molecular orbital models. J Am Chem Soc 130:10187–10198
31. Jones GO, Houk KN (2008) Predictions of substituent effects in thermal azide 1,3-dipolar cycloadditions: implications for dynamic combinatorial (reversible) and click (irreversible) chemistry. J Org Chem 73:1333–1342
32. Ess DH, Houk KN (2007) Distortion/interaction energy control of 1,3-dipolar cycloaddition reactivity. J Am Chem Soc 129:10646–10647
33. Ess DH, Jones GO, Houk NK (2006) Conceptual, qualitative, and quantitative theories of 1,3-dipolar and diels-alder cycloadditions used in synthesis. Adv Synth Catal 348:2337–2361
34. Jones GO, Ess DH, Houk KN (2005) Activation energies and reaction energetics for 1,3-dipolar cycloadditions of hydrazoic acid with C–C and C–N multiple bonds from high-accuracy and density functional quantum mechanical calculations. Helvetica Chimica Acta 88:1702–1710
35. Ess DH, Houk KN (2005) Activation energies of pericyclic reactions: performance of DFT, MP2, and CBS-QB3 methods for the prediction of activation barriers and reaction energetics of 1,3-dipolar cycloadditions, and revised activation enthalpies for a standard set of hydrocarbon pericyclic reactions. J Phys Chem A 109:9542–9553
36. Jung ME, Min S, Houk KN, Ess D (2004) Synthesis and relative stability of 3,5-diacyl-4,5-dihydro-1h-pyrazoles prepared by dipolar cycloaddition of enones and α-diazoketones. J Org Chem 69:9085–9089
37. Houk KN, Gonzalez J, Li Y (1995) Pericyclic reaction transition states: passions and punctilios, 1935–1995. Acc Chem Res 28:81–90
38. Gothelf KV, Jorgensen KA (1998) Asymmetric 1,3-dipolar cycloaddition reactions. Chem Rev 98:863–909
39. Kissane M, Maguire AR (2010) Asymmetric 1,3-dipolar cycloadditions of acrylamides. Chem Soc Rev 39:845–883
40. Xing Y, Wang N-X (2012) Organocatalytic and metal-mediated asymmetric (3 + 2) cycloaddition reactions. Coord. Chem. Rev. 256:938–952
41. Amblard F, Cho JH, Schinazi RF (2009) Cu(I)-catalyzed Huisgen azide-alkyne 1,3-dipolar cycloaddition reaction in nucleoside, nucleotide, and oligonucleotide chemistry. Chem Rev 109:4207–4220
42. Naodovi M, Yamamoto H (2008) Asymmetric silver-catalyzed reactions. Chem Rev 108:3132–3148
43. Stanley LM, Sibi MP (2008) Enantioselective copper-catalyzed 1,3-dipolar cycloadditions. Chem Rev 108:2887–2902
44. Lutz JF (2007) 1,3-dipolar cycloadditions of azides and alkynes: a universal ligation tool in polymer and materials science. Angew Chem Int Ed Engl 46:1018–1025
45. Tron GC, Pirali T, Billington RA, Canonico PL, Sorba G, Genazzani AA (2007) Click chemistry reactions in medicinal chemistry: applications of the 1,3-dipolar cycloaddition between azides and alkynes. Med Res Rev 28:278–308
46. Jewett J, Bertozzi CR (2010) Cu-free click cycloaddition reactions in chemical biology. Chem Soc Rev 39:1272–1279
47. Pieters RJ, Rijkers RMJ, Liskamp DTS (2007) Application of the 1,3-dipolar cycloaddition reaction in chemical biology: approaches toward multivalent carbohydrates and peptides and peptide-based polymers. QSAR Comb Sci 26:1181–1190
48. Huisgen R (1968) On the mechanism of 1,3-dipolar cycloadditions. A reply. J Org Chem 33:2291–2297
49. Firestone R (1968) On the mechanism of 1,3-dipolar cycloadditions. J Org Chem 33:2285–2290
50. Lan Y, Zou L, Cao Y, Houk KN (2011) Computational methods to calculate accurate activation and reaction energies of 1,3-dipolar cycloadditions of 24 1,3-dipoles. J Phys Chem A 115:13906–13920
51. Tantillo DJ, Lee JK (2011) Reaction mechanisms: pericyclic reactions. Annu Rep Prog Chem Sect B 107:266–286
52. Domingo LR, Picher T (2004) A DFT study of the Huisgen 1,3-dipolar cycloaddition between hindered thiocarbonyl ylides and tetracyanoethylene. Tetrahedron 60:5053–5058

53. Kraka E, Cremer D (2010) Computational analysis of the mechanism of chemical reactions in terms of reaction phases: hidden intermediates and hidden transition state. Acc Chem Res 43:591–601
54. Cremer D, Kraka E (2010) From molecular vibrations to bonding, chemical reactions, and reaction mechanism. Curr Org Chem 14:1524–1560
55. Konkoli Z, Cremer D, Kraka E (1997) Unified reaction valley approach: mechanism of the reaction $CH_3 + H_2 \rightarrow CH_4 + H$. J Phys Chem A 101:1742–1757
56. Kraka E (2011) Reaction path Hamiltonian and the unified reaction valley approach. In: Allen W, Schreiner PR (eds) Wiley interdisciplinary reviews: computational molecular science. Wiley, New York, pp 531–556
57. Kraka E (1998) Reaction path Hamiltonian and its use for investigating reaction mechanism. In: Schleyer PR, Allinger NL, Clark T, Gasteiger J, Kollman P, Schaefer HF, Schreiner PR (eds) Encyclopedia of computational chemistry, volume 4. Wiley, Chichester, p 2437
58. Miller WH, Handy NC, Adams JE (1980) Reaction path Hamiltonian for polyatomic molecules. J Chem Phys 72:99–112
59. Konkoli Z, Cremer D (1998) A new way of analyzing vibrational spectra I. Derivation of adiabatic internal modes. Int J Quant Chem 67:1–11
60. Konkoli Z, Cremer D (1998) A new way of analyzing vibrational spectra III. Characterization of normal vibrational modes in terms of internal vibrational modes. Int J Quant Chem 67:29–41
61. Kraka E, Larsson JA, Cremer D (1998) New developments in the analysis of vibrational spectra: on the use of adiabatic internal, vibrational modes. In: Parkanyi C (eds) Theoretical and computational chemistry, volume 5, theoretical organic chemistry, C. Elsevier, Amsterdam, p 259
62. Kraka E, Larsson JA, Cremer D (2010) Generalization of the badger rule based on the use of adiabatic vibrational modes. In: Grunenberg J (eds) Vibrational modes in computational IR spectroscopy. Wiley, New York, pp 105–149
63. Zou W, Kalesky R, Kraka E, Cremer D (2012) Relating normal vibrational modes to local vibrational modes with the help of an adiabatic connection scheme. J Chem Phys 137:084114–1–084114–11
64. Zou W, Kalescky R, Kraka E, Cremer D (2012) Relating normal vibrational modes to local vibrational modes benzene and naphthalene. J Mol Model 19:2865–2877
65. Cremer D, Wu A, Kraka E (2001) The mechanism of the reaction $FH + H_2C{=}CH_2 \rightarrow H_3C\text{-}CFH_2$. Investigation of hidden intermediates with the unified reaction valley approach. Phys Chem Chem Phys 3:674–687
66. Kraka E, Wu A, Cremer D (2003) Mechanism of the Diels–Alder reaction studied with the united reaction valley approach: mechanistic differences between symmetry-allowed and symmetry-forbidden reactions. J Phys Chem A 107:9008–9021
67. Kraka E, Joo H, Cremer D (2010) A stunning example for a spontaneous reaction with a complex mechanism: the vinylidene–acetylene cycloaddition reaction. Mol Phys 19(20):2667–2685
68. Joo H, Kraka E, Quapp W, Cremer D (2007) The mechanism of a barrierless reaction: hidden transition state and hidden intermediate in the reaction of methylene with ethene. Mol Phys 105:2697–2717
69. Kraka E, Zou W, Freindorf M, Cremer D (2012) Energetics and mechanism of the hydrogenation of XH_n for group IV to group VII elements X. J Chem Theory Comput 8:4931–4943
70. Raghavachari K, Trucks GW, Pople JA, Head-Gordon M (1989) A fifth-order perturbation comparison of electron correlation theories. Chem Phys Lett 157:479–483
71. Adler TB, Knizia G, Werner H-J (2007) A simple and efficient CCSD(T)-F12 approximation. J Chem Phys 127:221106–221110
72. Dunning T Jr (1989) Gaussian basis sets for use in correlated molecular calculations I. The atoms boron through neon and hydrogen. J Chem Phys 90:1007–1023
73. Fukui K (1981) The path of chemical reactions—the IRC approach. Acc Chem Res 14:363–368
74. Quapp W, Kraka E, Cremer D (2007) Finding the transition state of quasi-barrierless reactions by a growing string method for Newton trajectories: application to the dissociation of methylenecyclopropene and cyclopropane. J Chem Phys A 111:11287–11293
75. Hratchian HP, Kraka E (2013) Improved predictor-corrector integrators for evaluating reaction path curvature. J Chem Theor Comput 9:1481–1488
76. Becke AD (1993) Density-functional thermochemistry. III. The role of exact exchange. J Chem Phys 98:5648–5652
77. Stevens PJ, Devlin FJ, Chabalowski CF, Frisch MJ (1994) Ab initio calculation of vibrational absorption and circular dichroism spectra using density functional force fields. J Phys Chem 98:11623–11627
78. Hariharan PC, Pople JA (1973) The influence of polarization functions on molecular orbital hydrogenation energies. Theor Chimica Acta 28:213–222
79. Kraka E, Filatov M, Zou W, Gräfenstein J, Izotov D, Gauss J, He Y, Wu A, Polo V, Olsson L, Konkoli Z, He Z, Cremer D (2013) COLOGNE13
80. Reed AE, Curtiss LA, Weinhold F (1988) Intermolecular interactions from a natural bond orbital, donor-acceptor viewpoint. Chem Rev 88:899–926
81. Weinhold F, Landis CR (2003) Valency and bonding: a natural bond orbital donor–acceptor perspective. Cambridge University Press, Cambridge
82. Werner HJ, Knowles PJ, Kniza G, Manby FR, Schütz M, and others v MOLPRO, version 2010.1, a package of ab initio programs. see http://www.molpro.net
83. Chai J-D, Head-Gordon M (2008) Systematic optimization of long-range corrected hybrid density functionals. J Chem Phys 128:084106–1–084106–14
84. Chai J-D, Head-Gordon M (2008) Long-range corrected hybrid density functionals with damped atom–atom dispersion corrections. Phys Chem Chem Phys 10:6615–6620
85. Thanthiriwatte KS, Hohenstein EG, Burns LA, Sherrill CD (2011) Assessment of the performance of DFT and DFT-D methods for describing distance dependence of hydrogen-bonded interactions. J Chem Theor Comp 7:88–96
86. Boys SF, Bernardi F (1970) The calculation of small molecular interactions by the differences of separate total energies. Some procedures with reduced errors. Mol Phys 19:553–566
87. Cremer D, Pople JA (1975) A general definition of ring puckering coordinates. J Am Chem Soc 97:1354–1358
88. Cremer D, Szabo KJ (1995) Ab initio studies of six-membered rings, present status and future developments. In: Juaristi E (eds) Methods in stereochemical analysis, conformational behavior of six-membered rings, analysis, dynamics, and stereoelectronic effects. VCH Publishers, USA, pp 59–134
89. Cremer D, Izotov D, Zou W, Kraka E (2011) Southern Methodist University, Dallas, TX
90. Kraka E, Cremer D (2002) Mechanism and dynamics of organic reactions: 1,2-H shift in methylchlorocarbene. J Phys Org Chem 15:431–447
91. Hammond GS (1955) A correlation of reaction rates. J Am Chem. Soc 77:334–338
92. Leffler JE (1953) Parameters for the description of transition states. Science 117:340–341
93. Cremer D, Kraka E (2012) Verification and quantification of the Hammond–Leffler postulate. Rev Proc Quim: 27–30